Table S1. Overview of the individual HEGITOM sites that are included in the LMM synthesized trend estimation for each region. The instrument type, site/airport name or code, latitude, longitude, begin and end year of the time series since 1990 and the total number of observations during this time period are shown.

Region	Instrument	Name	lat	lon	begin	end	N_{obs}
Europe	O3S	Madrid	40.47	-3.58	1994	2022	1179
Europe	O3S	L'Aquila	42.30	13.31	1994	2023	354
Europe	Lidar	OHPO3T	43.94	5.71	2000	2022	1592
Europe	O3S	OHPO3T	43.94	5.71	1991	2023	1494
Europe	Umk	40	43.94	5.71	1985	2022	6037
Europe	O3S	Payerne	46.49	6.57	2002	2022	3112
Europe	FTIR	Jungfraujoch	46.55	7.98	2000	2023	8649
Europe	Umk	35	46.78	9.68	1979	2022	4731
Europe	FTIR	Zugspitze	47.42	10.98	1995	2022	20113
Europe	O3S	Hohenpeissenberg	47.80	11.01	1966	2023	6438
Europe	IAGOS	VIE	48.12	16.56	1995	2021	3929
Europe	IAGOS	MUC	48.35	11.79	1996	2011	1995
Europe	IAGOS	CDG	49.00	2.57	1994	2022	4661
Europe	IAGOS	FRA	50.05	8.57	1994	2022	18457
Europe	O3S	Uccle	50.80	4.35	1969	2022	6717
Europe	IAGOS	BRU	50.90	4.48	1997	2009	2121
Europe	IAGOS	LGW	51.16	-0.16	2005	2009	378
Europe	IAGOS	DUS	51.28	6.77	1995	2015	984
Europe	O3S	Valentia	51.94	-10.25	1994	2022	767
Europe	O3S	De Bilt	52.10	5.18	1992	2020	1487
Europe	O3S	Legionowo	52.40	20.97	1993	2022	1744
Europe	FTIR	Bremen	53.10	8.85	2004	2023	1994
Eur Arctic	O3S	Lerwick	60.13	-1.18	1992	2022	1631
Eur Arctic	FTIR	Harestua	60.20	10.80	2009	2020	2366
Eur Arctic	O3S	Sodankylä	67.37	26.65	1994	2022	1434
Eur Arctic	FTIR	Kiruna	67.84	20.40	1996	2022	5461
Eur Arctic	O3S	Scoresbysund	70.48	-21.97	1989	2022	1587
Eur Arctic	FTIR	Ny Ålesund	78.92	11.92	1994	2022	2457
Eur Arctic	O3S	Ny Ålesund	78.92	11.93	1992	2022	2632
Can Arctic	O3S	Resolute	74.70	-94.96	1966	2021	2182
Can Arctic	FTIR	Thule	76.53	-68.74	1999	2022	6210
Can Arctic	O3S	Eureka	79.98	-85.94	1992	2021	1870
Can Arctic	FTIR	Eureka	80.05	-86.42	2006	2020	6261
Can Arctic	O3S	Alert	82.49	-62.34	1987	2020	1587
California	IAGOS	LAX	33.94	-118.41	1995	2018	270
California	Lidar	TMF	34.38	-117.68	2000	2023	2918
California	IAGOS	SFO	37.62	-122.39	1994	2018	331
W USA	IAGOS	LAX	33.94	-118.41	1995	2018	270
W USA	Lidar	TMF	34.38	-117.68	2000	2023	2918
W USA	IAGOS	SFO	37.62	-122.39	1994	2018	331
W USA	Umk	67	39.99	-105.26	1979	2022	7093

W USA	O3S	Boulder	40.00	-105.25	1967	2023	2037
W USA	FTIR	Boulder	40.04	-105.24	2010	2022	3613
Pacific NW	IAGOS	PDX	45.59	-122.59	2003	2018	380
Pacific NW	IAGOS	YVR	49.19	-123.18	1995	2021	596
Pacific NW	O3S	Kelowna	49.93	-119.40	2003	2017	699
Pacific NW	O3S	Port Hardy	50.68	-127.38	2018	2021	109
Pacific NW	O3S	Edmonton	53.54	-114.10	1970	2021	2169
E N America	O3S	Wallops Island	37.93	-75.48	1995	2020	1474
E N America	IAGOS	IAD	38.95	-77.45	1994	2022	689
E N America	IAGOS	PHL	39.88	-75.24	1999	2022	713
E N America	IAGOS	JFK	40.64	-73.79	1994	2022	2222
E N America	IAGOS	EWR	40.69	-74.18	1994	2021	1151
E N America	IAGOS	ORD	41.98	-87.90	1994	2021	1343
E N America	IAGOS	DTW	42.21	-83.36	1999	2022	454
E N America	IAGOS	BOS	42.37	-71.02	1994	2022	1137
E N America	FTIR	Toronto	43.60	-79.36	2002	2023	5497
E N America	IAGOS	YYZ	43.68	-79.61	1994	2021	870
E N America	O3S	Yarmouth	43.87	-66.11	2003	2021	793
E N America	IAGOS	YUL	45.46	-73.75	1999	2021	276
E N America	O3S	Goose Bay	53.31	-60.36	1969	2021	2351
SE US	IAGOS	IAH	29.98	-95.34	1994	2022	570
SE US	IAGOS	DAL	32.84	-96.85	1995	2022	1263
SE US	IAGOS	ATL	33.64	-84.44	1994	2022	1948
East China	IAGOS	PVG	31.15	121.80	2000	2021	182
East China	IAGOS	SHA	31.20	121.34	1997	2000	200
East China	IAGOS	NKG	31.74	118.87	2009	2020	69
East China	FTIR	Hefei	31.91	117.17	2015	2020	3375
S Japan	IAGOS	KIX	34.44	135.24	1994	2018	1209
S Japan	IAGOS	NGO	34.86	136.81	2006	2020	413
S Japan	IAGOS	NKM	35.25	136.92	1997	2004	86
S Japan	IAGOS	NRT	35.77	140.39	1995	2018	1170
S Japan	FTIR	Tsukuba	36.05	140.12	2014	2020	780
NE Asia	IAGOS	TAO	36.27	120.38	2012	2022	127
NE Asia	IAGOS	ICN	37.45	126.45	2001	2022	171
NE Asia	IAGOS	GMP	37.56	126.80	1994	2000	260
NE Asia	IAGOS	PEK	40.08	116.59	1995	2021	766
NE Asia	IAGOS	SHE	41.86	123.43	2012	2021	219
NE Asia	FTIR	Rikubetsu	43.46	143.77	1995	2022	2670
NE Asia	FTIR	Moshiri	44.40	142.30	1996	2007	1473
SE Asia	IAGOS	SGN	10.81	106.66	1994	2018	239
SE Asia	IAGOS	BKK	13.69	100.75	2006	2022	272
SE Asia	IAGOS	DMK	13.91	100.61	1994	2006	748
S China Sea	O3S	Hanoi	21.01	105.80	2004	2021	350
S China Sea	IAGOS	HAN	21.21	105.80	1994	2018	117
S China Sea	IAGOS	HKG	22.32	113.94	1999	2021	728

S China Sea	IAGOS	CAN	23.39	113.30	2005	2018	94
S China Sea	IAGOS	TPE	25.08	121.22	2012	2018	1422
S Malay Peninsula	IAGOS	SIN	1.36	103.99	1995	2022	170
S Malay Peninsula	O3S	Kuala Lumpur	2.73	101.27	1998	2022	498
S Malay Peninsula	IAGOS	KUL	2.76	101.71	1998	2016	87
India	IAGOS	MAA	12.98	80.16	1994	2018	460
India	IAGOS	HYD	17.24	78.43	2005	2018	485
Persian Gulf	IAGOS	JED	21.67	39.15	1999	2019	240
Persian Gulf	IAGOS	AUH	24.43	54.65	1999	2017	67
Persian Gulf	IAGOS	RUH	24.96	46.70	1999	2022	288
Persian Gulf	IAGOS	DXB	25.25	55.35	1997	2022	538
Persian Gulf	IAGOS	DOH	25.27	51.56	2012	2017	131
Persian Gulf	IAGOS	BAH	26.27	50.63	2010	2021	14
Persian Gulf	IAGOS	DMM	26.47	49.80	2003	2022	68
Persian Gulf	IAGOS	KWI	29.24	47.97	2001	2022	417
Gulf of Guinea	IAGOS	SSG	3.76	8.72	2014	2022	126
Gulf of Guinea	IAGOS	DLA	4.01	9.72	1997	2022	141
Gulf of Guinea	IAGOS	PHC	5.01	6.95	2002	2022	79
Gulf of Guinea	IAGOS	ABJ	5.25	-3.93	1997	2022	187
Gulf of Guinea	IAGOS	ACC	5.61	-0.17	2003	2022	45
Gulf of Guinea	IAGOS	LFW	6.17	1.25	1997	2022	63
Gulf of Guinea	IAGOS	COO	6.35	2.39	2001	2022	68
Gulf of Guinea	IAGOS	LOS	6.58	3.32	1997	2022	494
Gulf of Guinea	IAGOS	ABV	9.00	7.27	2003	2022	247
Hawaii	O3S	Hilo	19.43	-155.04	1982	2023	1829
Hawaii	FTIR	Mauna Loa	19.54	-155.57	1995	2022	10226
Hawaii	Umk	31	19.54	-155.58	1985	2022	11971
Oceania	FTIR	Lauder	-45.04	169.68	2001	2023	10389
Oceania	Umk	256	-45.04	169.68	1987	2022	4233
Oceania	O3S	Lauder	-45.00	169.68	1986	2021	1810
Oceania	FTIR	Wollongong	-34.41	150.88	2007	2023	8481

Table S2: Synthesized TrOC trend estimates. 2-sigma uncertainties. p-values. and trend confidence for the different regions for 1995-2019 (colums (1) to (3)). and for 2000-2019 (columns (4) to (6)). Following the TOAR-II statistical guidelines (Chang et al., 2023) the following degrees of certainty is assigned to a trend according to p value: very high certainty ($p \leq 0.01$). high certainty ($0.05 \geq p > 0.01$). medium certainty ($0.10 \geq p > 0.05$). low certainty ($0.33 \geq p > 0.10$). and very low certainty or no evidence ($p > 0.33$). Combining these uncertainty levels with the data coverage assignments in Table 2 gives the calibrated language for discussing confidence in long-term trend estimates as in Gaudel et al. (2024). and included here in columns (3) and (6).

	(1)	(2)	(3)	(4)	(5)	(6)
	1995-2019			2000-2019		
	Trend ± 2σ [ppb/dec]	p-value	confidence	Trend ± 2σ [ppb/dec]	p-value	confidence
Europe	0.47±0.20	<0.01	very high	0.60±0.29	<0.01	very high
Eur Arctic	-0.30±0.31	0.06	high	-0.97±0.46	<0.01	very high
Can Arctic	-0.48±0.52	0.06	high	-0.45±0.65	0.16	medium
California	2.60±0.91	<0.01	high	2.16±0.93	<0.01	high
W USA	1.13±0.57	<0.01	very high	0.83±0.69	0.02	very high
Pacific NW	0.04±0.58	0.88	low	-0.10±0.74	0.78	low
E N America	0.17±0.45	0.45	low	-0.54±0.55	0.05	high
SE US	1.17±0.81	<0.01	high	0.73±1.12	0.19	low
E China	5.10±2.39	<0.01	high	4.04±3.79	0.03	high
S Japan	1.69±0.97	<0.01	medium	1.81±1.28	<0.01	medium
NE Asia	1.73±0.95	<0.01	high	0.86±1.04	0.10	medium
SE Asia	5.74±1.24	<0.01	medium	2.68±2.49	0.03	medium
S China Sea	4.75±1.29	<0.01	medium	3.79±1.72	<0.01	medium
S Malay Peninsula	3.36±1.02	<0.01	medium	2.99±1.17	<0.01	medium
India	6.07±1.41	<0.01	medium	6.08±2.28	<0.01	medium
Persian Gulf	2.25±0.87	<0.01	medium	2.11±0.94	<0.01	medium
Gulf of Guinea	1.16±0.71	<0.01	medium	0.99±0.80	0.01	medium
Hawaii	0.62±0.40	<0.01	very high	0.71±0.58	0.01	very high
Oceania	0.65±0.31	<0.01	very high	0.98±0.40	<0.01	very high

Table S3: Same as Table S2, but now for the FTOC and the post-COVID (1995-2022) and pre-COVID (1995-2019) time periods. Also note that the Hawaii and Oceania regions had to be discarded, because they only rely on ozone ozonesonde time series for the FTOC, as the FTIR and Umkehr instruments only provide the entire tropospheric ozone column TrOC. As for India, the time series of the two IAGOS sites only extend up to 2018, only 1995-2019 trends are listed here. In the text and figures, these values have been used for the 1995-2022 trends as well.

	(1)	(2)	(3)	(4)	(5)	(6)
	1995-2022			1995-2019		
	Trend ± 2σ [ppb/dec]	p-value	confidence	Trend ± 2σ [ppb/dec]	p-value	confidence
Europe	0.68±0.23	<0.01	very high	1.25±0.27	<0.01	very high
Eur Arctic	-1.00±0.47	<0.01	very high	-0.18±0.52	0.49	medium
Can Arctic	-1.00±0.81	0.01	high	-0.72±0.86	0.09	medium
California	1.93±0.79	<0.01	high	2.38±0.97	<0.01	high
W USA	0.45±0.97	0.35	low	0.62±1.01	0.22	low
Pacific NW	0.20±0.73	0.59	low	0.29±0.78	0.46	low
E N America	0.17±0.55	0.54	low	0.53±0.60	0.08	medium
SE US	1.41±0.78	<0.01	high	1.52±0.91	<0.01	high
E China	1.21±2.15	0.26	very low	1.09±2.38	0.36	very low
S Japan	1.12±1.13	0.05	medium	1.18±1.13	0.04	medium
NE Asia	2.62±0.91	<0.01	medium	2.74±0.92	<0.01	medium
SE Asia	4.91±1.22	<0.01	medium	4.88±1.22	<0.01	medium
S China Sea	3.76±1.20	<0.01	medium	4.54±1.34	<0.01	medium
S Malay Peninsula	1.37±0.91	<0.01	medium	2.22±1.10	<0.01	medium
India				4.95±1.42	<0.01	medium
Persian Gulf	1.10±0.85	0.01	medium	1.52±0.95	<0.01	medium
Gulf of Guinea	-0.48±0.67	0.16	very low	0.01±0.84	0.99	very low

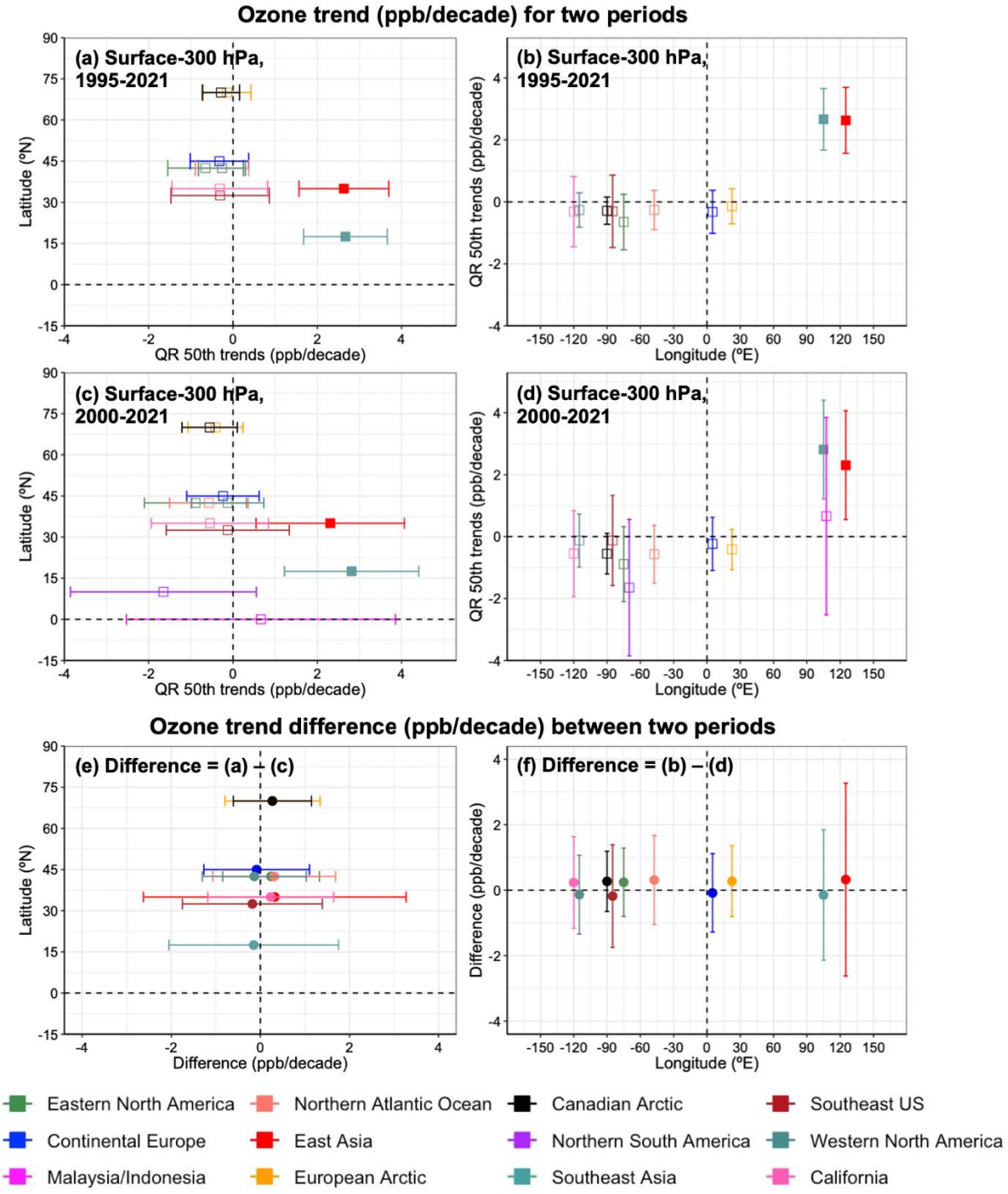

Fig. S1: (a, b) TOST QR Median trends (in ppb/decade) of the mean ozone mixing ratios from surface-300 hPa varying with latitude (left) and longitude (right), for the period of 1995-2021. Error bars represent the 95% confidence interval of the QR trend. Colors denote the regions. (c, d) The same as (a, b), but for the period of 2000-2021. (e, f). The difference in the QR median trend between the periods of 1995-2021 and 2000-2021. Error bars represent the 95% confidence interval for the QR median trend difference.

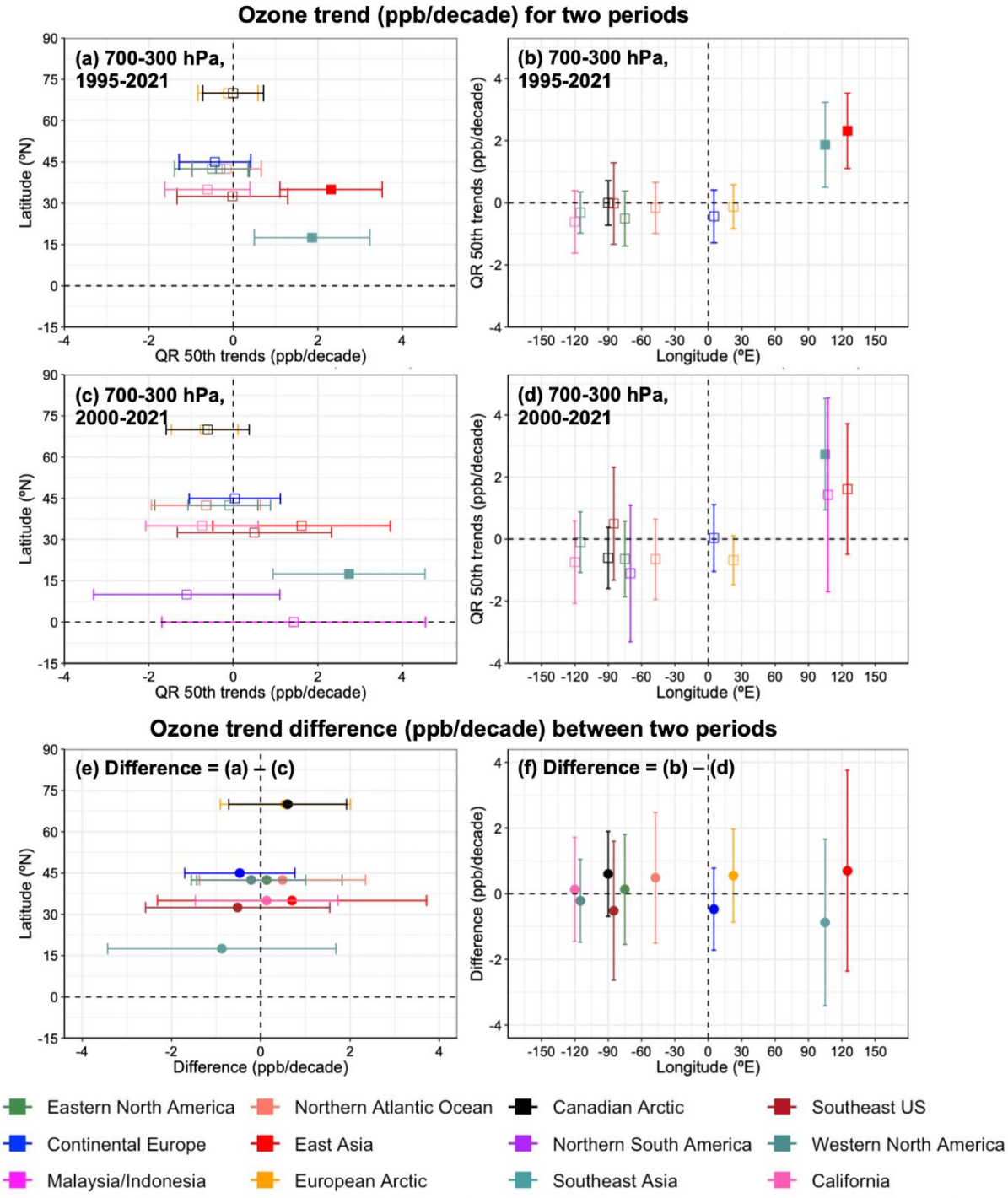

Fig. S2: The same as Fig. 7, but for the mean ozone mixing ratio over 700-300 hPa, FTOC.

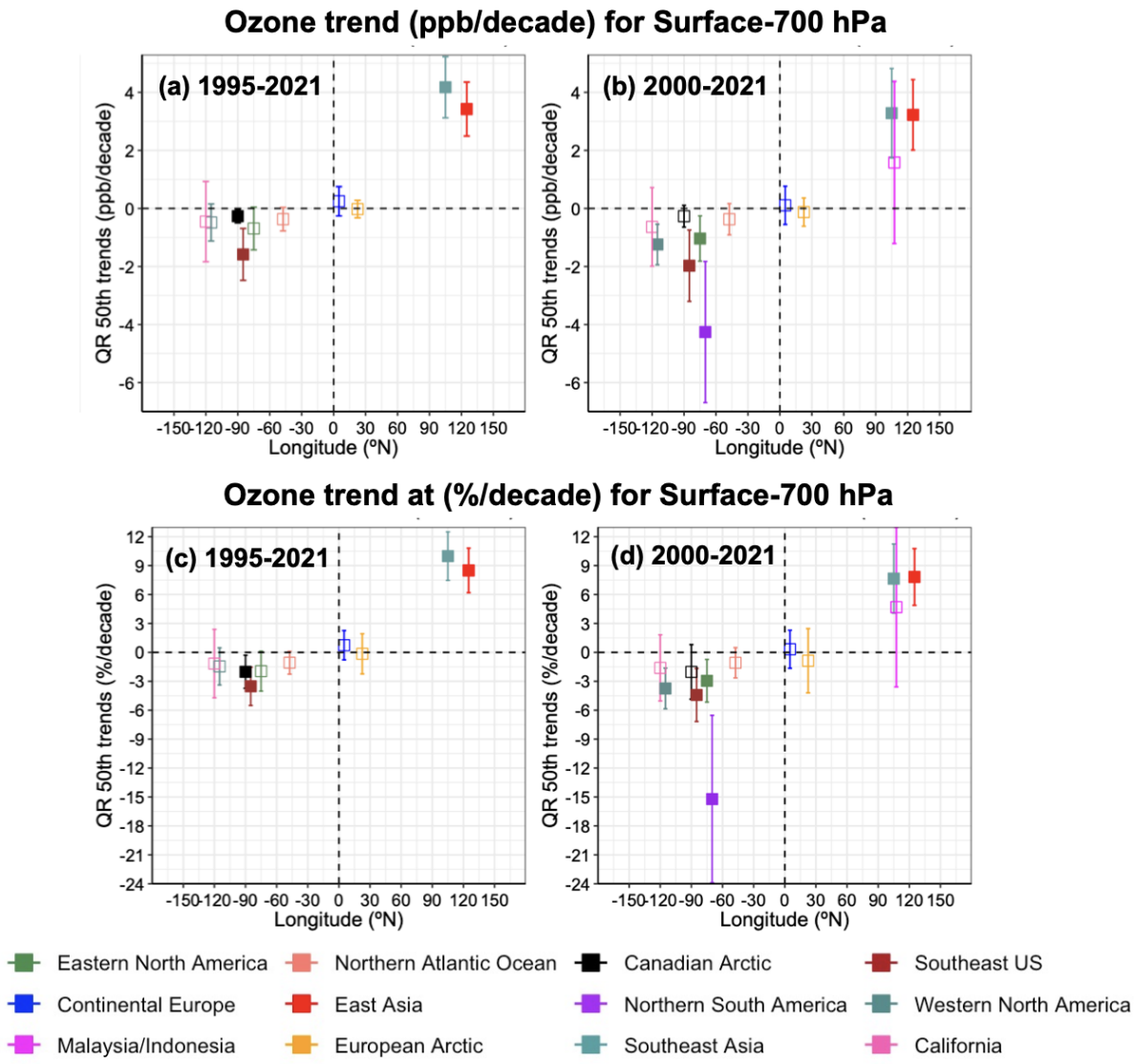

Fig. S3: (a, b). TOST QR median trends (in ppb/decade) of the mean ozone mixing ratios from surface-700 hPa (LTOC) varying with longitude, for the periods of 1995-2021 and 2000-2021. Error bars represent the 95% confidence interval for the QR trend. Colors denote the regions. (c, d). The same as (a, b), but for the relative QR median trends in %/decade.

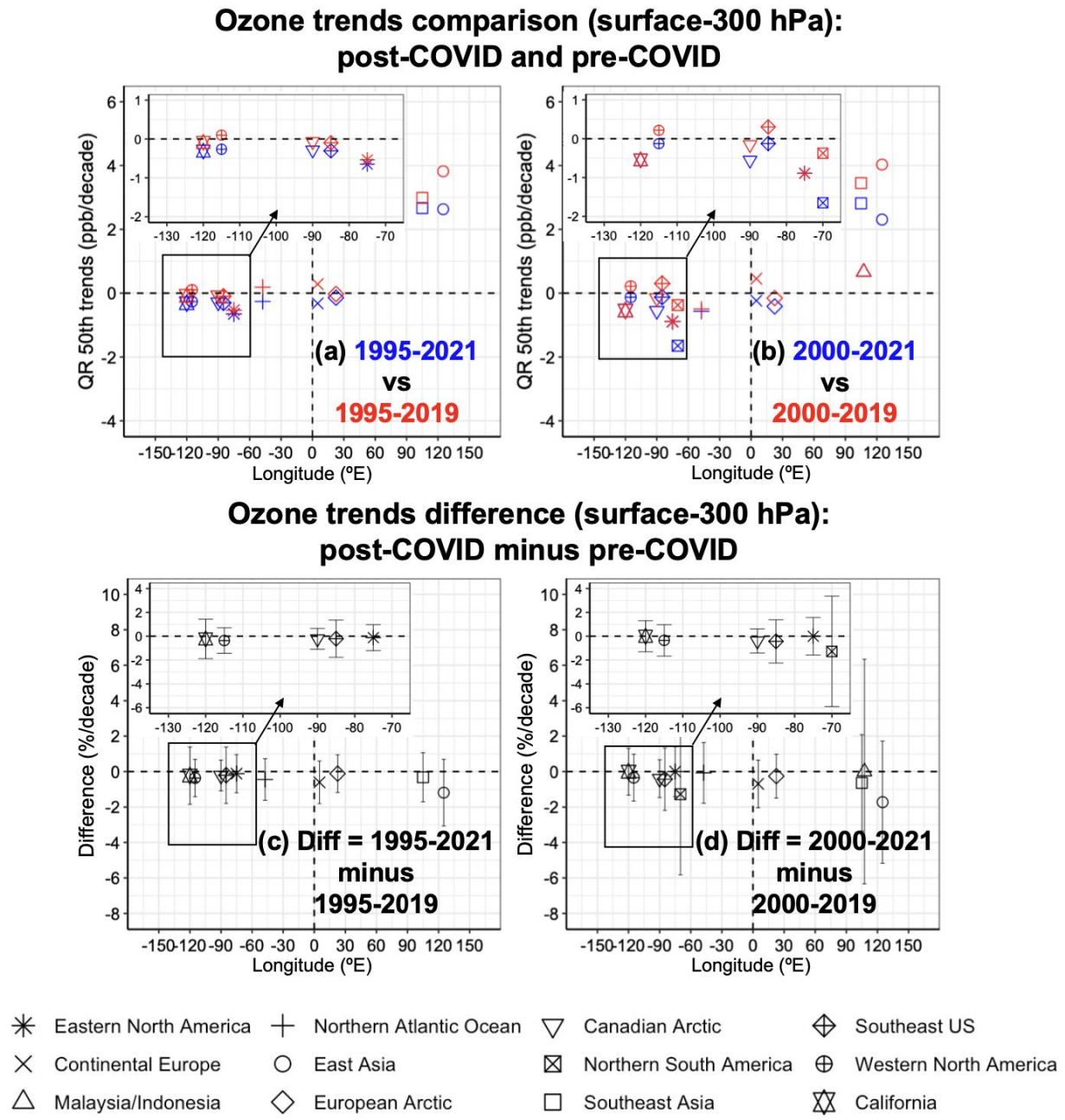

Fig. S4: (a). TOST QR median absolute trends (in ppb/decade) of the mean ozone mixing ratios from surface-300 hPa varying with longitude, for the periods 1995-2021 and 1995-2019. Shapes denote the regions. (b). The same as (a), but for the periods 2000-2021 and 2000-2019. (c). QR Median trend difference between the periods 1995-2021 and 1995-2019. Error bars represent the 95% confidence interval for the QR Median trend difference. (d). The same as (c), but between the periods 2000-2021 and 2000-2019. All zoom-in windows are to show the trends in North America more clearly.

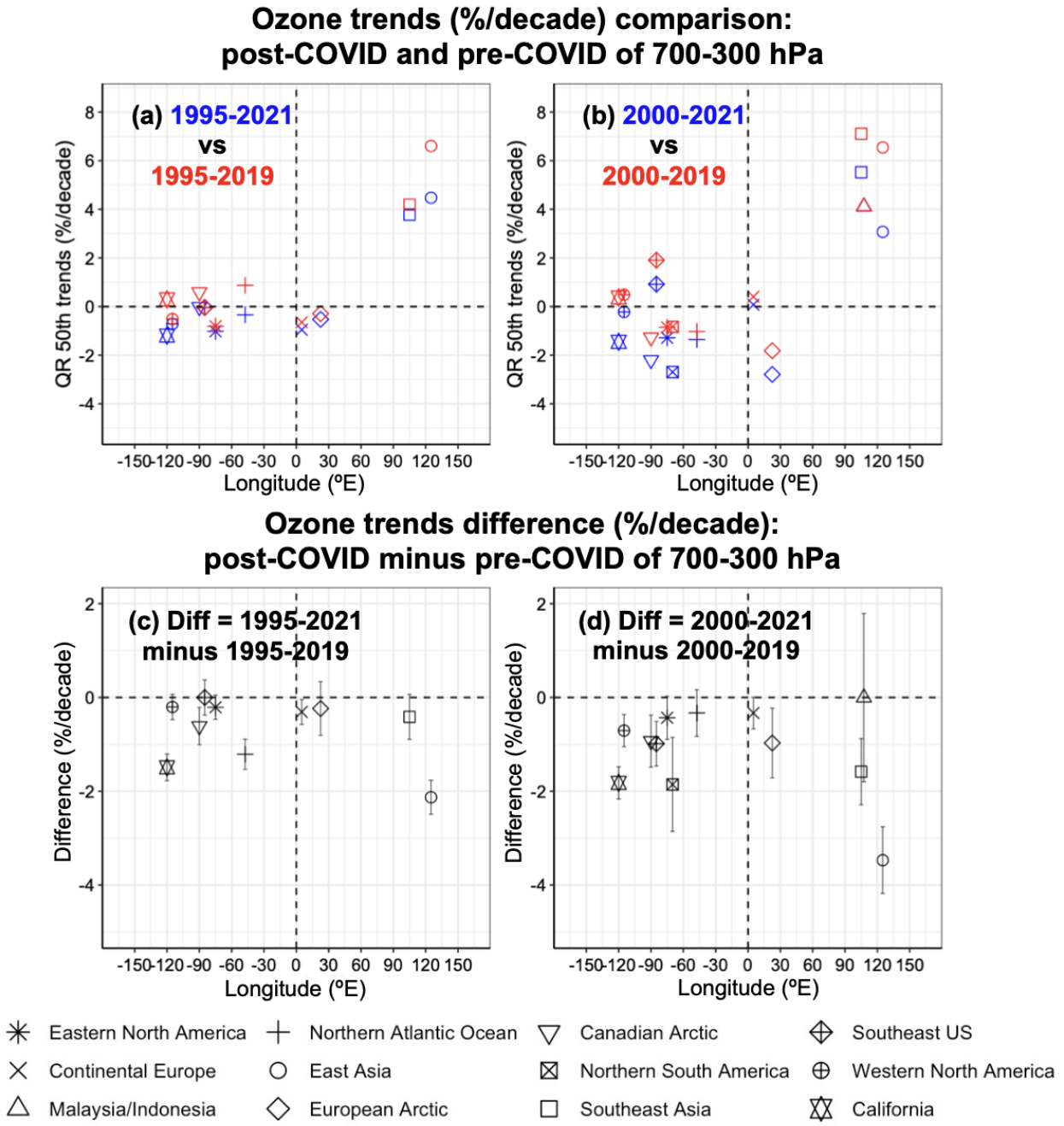

Fig. S5: The same as Fig. 9, but now for TOST QR median relative trends (in %/decade) for the mean ozone mixing ratio from 700-300 hPa, FTOC.

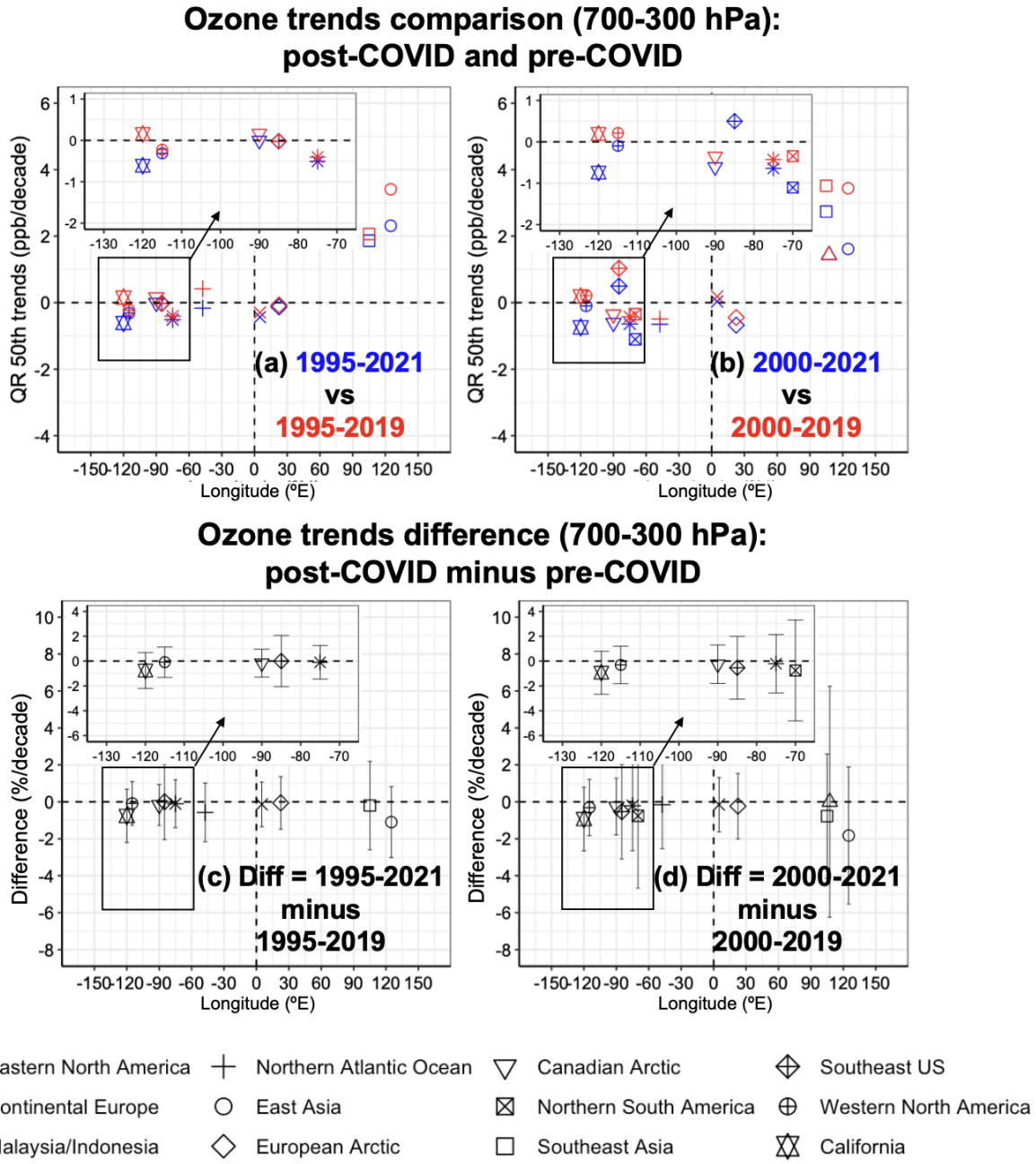

Fig. S6: The same as Fig. S5, but now for TOST QR median absolute trends (in ppb/decade) for the mean ozone mixing ratio from 700-300 hPa, FTOC.

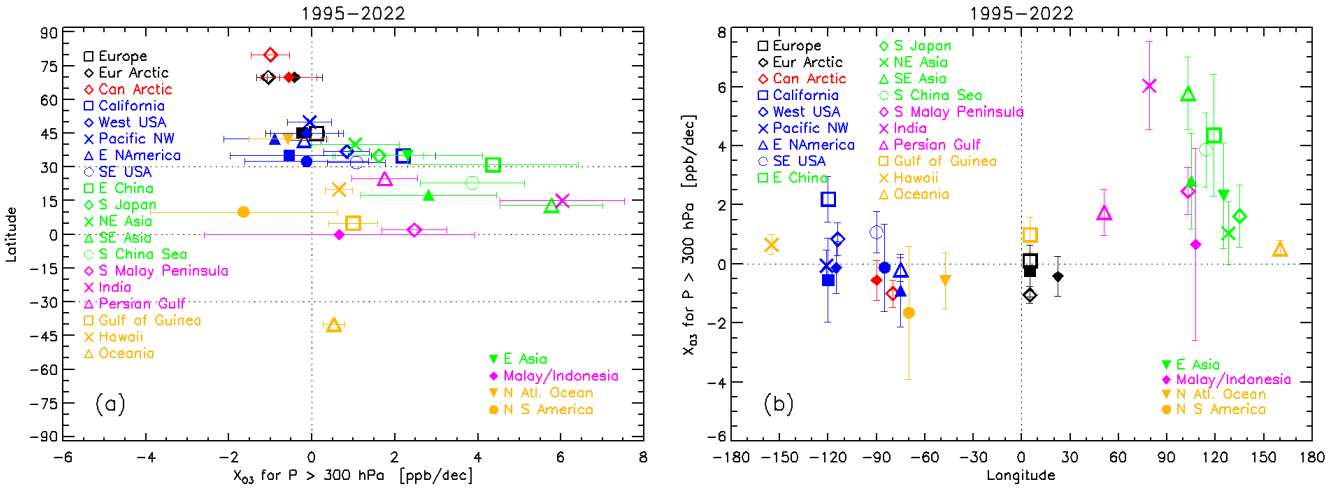

Fig. S7: Same as Fig 13, but <u>now for the 1995-2021/22 period</u>, and without including the individual site QR trend estimates, as they have been calculated only for the 2000-2022 period.

Section S1 Example R code for deriving synthesized trends using the linear mixed-effects modelling approach

This section provides an example R code of deriving the synthesized trends, based on 9 sites in the European Arctic region. To apply this code to other regions, uncertainty values associated with different instrumental types need to be updated accordingly.

```
########################################################################
#European Arctic
########################################################################
set.seed(2013)
library(mgcv)
filename=c("IAGOS_HEL_1997_1997_L1_v2.csv",
        "IAGOS_KEF_2003_2013_L1_v2.csv",
        "O3S_nyalesund_1992_2022_L1_v3.csv",
        "O3S_scoresbysund_1989_2022_L1_v3.csv",
        "O3S_sodankyla_1994_2022_L1_v3.csv",
        "O3S_lerwick_1992_2022_L1_v3.csv",
        "FTIR_Kiruna_1996_2022_L1_v1.csv",
        "FTIR_Ny_Alesund_1994_2022_L1_v1.csv",
        "FTIR_Harestua_2009_2020_L1_v1.csv")
nm=12*(2022-1990+1)
ny=2022-1965+1

datalist=lapply(filename[1:9], function(x) read.csv(x))
for (i in 1:length(datalist)){
  datalist[[i]]$site=i
  datalist[[i]]=datalist[[i]][,c("year", "month", "day", "hour", "XO3_p300", "site")]
}
dt = do.call("rbind", datalist)

#data reformatting
date=cbind(month=rep(seq(1,12),ny), year=rep(seq(1965,2022), each=12), ind=seq(1,12*ny))
dt=merge(dt,date, by=c("year","month"), all.x=T)
time=seq(from=as.Date("1965-01-01"), to=as.Date("2022-12-31"), by=1)
date2=cbind(year=format(time, format="%Y"), month=format(time, format="%m"), day=format(time, format="%d"),
indd=seq(1,length(time)))
date2=apply(date2, 2, as.numeric)
dt=merge(dt, date2, by=c("year","month","day"), all.x=T)
dt=merge(dt, enso, by=c("year","month"), all.x=T)
dt=dt[order(dt$indd),]
dt[dt<=-999]=NA

#the main function to derive the synthesized trends
#note: uncertainty values are dependent on the instrumental types
mbfun.gamm.dataunc=function(formula,data){
  n=nrow(data)
  b=ceiling(n^0.25)
  nblocks=ceiling(n/b)
  blocks=lapply(seq_len(n-b+1), function(i) seq(i, i+b-1))
  bn=sample(1:length(blocks),nblocks,replace=T)
  sdt=data[unlist(blocks[bn]), ]
  sdt[sdt$site==1,"XO3_p300"]=sdt[sdt$site==1,"XO3_p300"]+rnorm(length(sdt[sdt$site==1,"XO3_p300"]), mean=0,
sd=sdt[sdt$site==1,"XO3_p300"]*0.055)
  sdt[sdt$site==2,"XO3_p300"]=sdt[sdt$site==2,"XO3_p300"]+rnorm(length(sdt[sdt$site==2,"XO3_p300"]), mean=0,
sd=sdt[sdt$site==2,"XO3_p300"]*0.055)
  sdt[sdt$site==3,"XO3_p300"]=sdt[sdt$site==3,"XO3_p300"]+rnorm(length(sdt[sdt$site==3,"XO3_p300"]), mean=0,
sd=sdt[sdt$site==3,"XO3_p300"]*0.055)
  sdt[sdt$site==4,"XO3_p300"]=sdt[sdt$site==4,"XO3_p300"]+rnorm(length(sdt[sdt$site==4,"XO3_p300"]), mean=0,
sd=sdt[sdt$site==4,"XO3_p300"]*0.055)
```

```
  sdt[sdt$site==5,"XO3_p300"]=sdt[sdt$site==5,"XO3_p300"]+rnorm(length(sdt[sdt$site==5,"XO3_p300"]), mean=0,
sd=sdt[sdt$site==5,"XO3_p300"]*0.055)
  sdt[sdt$site==6,"XO3_p300"]=sdt[sdt$site==6,"XO3_p300"]+rnorm(length(sdt[sdt$site==6,"XO3_p300"]), mean=0,
sd=sdt[sdt$site==6,"XO3_p300"]*0.055)
  sdt[sdt$site==7,"XO3_p300"]=sdt[sdt$site==7,"XO3_p300"]+rnorm(length(sdt[sdt$site==7,"XO3_p300"]), mean=0,
sd=sdt[sdt$site==7,"XO3_p300"]*0.14)
  sdt[sdt$site==8,"XO3_p300"]=sdt[sdt$site==8,"XO3_p300"]+rnorm(length(sdt[sdt$site==8,"XO3_p300"]), mean=0,
sd=sdt[sdt$site==8,"XO3_p300"]*0.14)
  sdt[sdt$site==9,"XO3_p300"]=sdt[sdt$site==9,"XO3_p300"]+rnorm(length(sdt[sdt$site==9,"XO3_p300"]), mean=0,
sd=sdt[sdt$site==9,"XO3_p300"]*0.14)
  sdt=aggregate(.~ind+site, data=sdt, FUN=function(x) {mean(x,na.rm=T)})
  tryCatch({mod=gamm(formula, random=list(site=~1+ind), data=sdt)
  coef(mod$gam)
  }, error=function(e){})
}

start.year=pmax(min(dt$year, na.rm=T), 1990)
if (start.year<1995 & length(unique(dt$year))>15){
  pt=dt[dt$year>=1990,]
  mod=replicate(1000, mbfun.gamm.dataunc(formula=XO3_p300~ind+s(month,bs="cc",k=12)+enso,data=pt))
  if (is.list(mod)) {mod=t(do.call("rbind", mod))}
  trend=mean(mod[2,])*120
  trend.unc=sd(mod[2,])*120
  pvalue=2*pt(q=abs(trend/trend.unc), df=nrow(pt)-14, lower.tail=FALSE)
}
```